

**Weierstraß-Institut**  
**für Angewandte Analysis und Stochastik**  
**Leibniz-Institut im Forschungsverbund Berlin e. V.**

Preprint

ISSN 2198-5855

**Regular triangulation and power diagrams**  
**for Maxwell's equations**

Rainer Schlundt

submitted: October 6, 2014

Weierstrass Institute  
Mohrenstr. 39  
10117 Berlin  
Germany  
E-Mail: rainer.schlundt@wias-berlin.de

No. 2017  
Berlin 2014



---

2010 *Mathematics Subject Classification.* 35Q61, 65F10, 65F15, 65N22, 65N50.

*Key words and phrases.* Maxwell's equations, finite integration technique, linear algebraic equations, eigenvalue problem, optimal triangulations, discrete Hodge star, microcell method.

Edited by  
Weierstraß-Institut für Angewandte Analysis und Stochastik (WIAS)  
Leibniz-Institut im Forschungsverbund Berlin e. V.  
Mohrenstraße 39  
10117 Berlin  
Germany

Fax: +49 30 20372-303  
E-Mail: [preprint@wias-berlin.de](mailto:preprint@wias-berlin.de)  
World Wide Web: <http://www.wias-berlin.de/>

## Abstract

We consider the solution of electromagnetic problems. A mainly orthogonal and locally barycentric dual mesh is used to discretize the Maxwell's equations using the Finite Integration Technique (FIT). The use of weighted duals allows greater flexibility in the location of dual vertices keeping the primal-dual orthogonality. The construction of the constitutive matrices is performed using either discrete Hodge stars or microcells. Hodge-optimized triangulations (HOT) can optimize the dual mesh alone to make it more self-centered while maintaining the primal-dual orthogonality, e.g., the weights are optimized in order to improve one or more of the discrete Hodge stars.

## 1 Introduction

We consider the Maxwell's equations in integral form. Also we define differential forms of various degrees and identify them with field intensity, flux density, charge density, and scalar potential. A significant advantage of the calculus of differential forms over traditional methods is that forms clarify the relationship between field intensity and flux density. A differential form is a quantity that can be integrated, including differentials (cf. [13]).

From Maxwell's equations in integral form, we can readily determine the degrees of the differential forms. We obtain in vector notation the following equations:

$$\oint_P \mathbf{E} \cdot d\mathbf{l} = -\frac{\partial}{\partial t} \iint_A \mathbf{B} \cdot d\mathbf{A} \quad (1a)$$

$$\oint_P \mathbf{H} \cdot d\mathbf{l} = \frac{\partial}{\partial t} \iint_A \mathbf{D} \cdot d\mathbf{A} + \iint_A \mathbf{J} \cdot d\mathbf{A} \quad (1b)$$

$$\oiint_S \mathbf{D} \cdot d\mathbf{S} = \iiint_V q \, dV \quad (1c)$$

$$\oiint_S \mathbf{B} \cdot d\mathbf{S} = 0. \quad (1d)$$

The constitutive relations belonging to them are

$$\mathbf{D} = \varepsilon \mathbf{E} \quad (2a)$$

$$\mathbf{B} = \mu \mathbf{H} \quad (2b)$$

$$\mathbf{J} = \kappa \mathbf{E}. \quad (2c)$$

Here,  $A$  is a surface by a path  $P$ ,  $V$  is a volume bounded by a surface  $S$ , and  $q$  is the volume charge density. The electric and magnetic field intensities are integrated over paths and become 1-forms. The electric and magnetic flux densities are integrated over surfaces and so are 2-forms. The electric current density is also a 2-form since it falls under a surface integral. The volume charge density is a 3-form since it is integrated over a volume. Table 1 summarizes these forms.

Table 1: Electromagnetic quantities and differential forms.

Quantity	Form	Degree	Unit	Vector/Scalar
electric potential	$\varphi$	0-form	$V$	$\phi$
electric field intensity	$E$	1-form	$V/m$	$\mathbf{E}$
magnetic field intensity	$H$	1-form	$A/m$	$\mathbf{H}$
electric flux density	$D$	2-form	$C/m^2$	$\mathbf{D}$
magnetic flux density	$B$	2-form	$Wb/m^2$	$\mathbf{B}$
electric current density	$J$	2-form	$A/m^2$	$\mathbf{J}$
electric charge density	$\rho$	3-form	$C/m^3$	$q$

In Section 2, we first give some background on regular triangulations and power diagrams - the dual structure of regular triangulations. In Section 3, we discretize the Maxwell's equations and the constitutive relations. In Section 4, we introduce Hodge-optimized triangulations (HOT), a family of primal-dual pairs of complexes. Tests in Section 5 show that optimizing the weights reduce the number of negative dual edges.

## 2 Regular triangulation and power diagrams

The regular triangulation is a generalization of well-known Delaunay triangulation. First we start with the definition of a  $k$ -simplex. A  $k$ -simplex  $\sigma^k$  is the convex hull of  $k + 1$  geometrically independent points  $\mathbf{x}_1, \dots, \mathbf{x}_{k+1} \in \mathbb{R}^d$  with  $d \in \{0, 1, 2, 3\}$  and  $0 \leq k \leq d$ .

$$\sigma^k = \left\{ \mathbf{z} \in \mathbb{R}^d : \mathbf{z} = \sum_{i=1}^{k+1} \lambda_i \mathbf{x}_i, 0 \leq \lambda_i \leq 1, \sum_{i=1}^{k+1} \lambda_i = 1 \right\} \quad (3)$$

Any simplex spanned by a proper subset of  $\{\mathbf{x}_1, \dots, \mathbf{x}_{k+1}\}$  is called a face of  $\sigma^k$ . The union of the proper faces of  $\sigma^k$  is called its boundary. The interior of  $\sigma^k$  is the set difference of  $\sigma^k$  and its boundary. The interior of  $\sigma^0$  is  $\sigma^0$ . The volume of  $\sigma^k$  is denoted by  $|\sigma^k|$ . Define  $|\sigma^0| = 1$  (cf. [7]).

Given a set of points  $S \subset \mathbb{R}^d$ . The triangulation  $\mathcal{T}(S)$  of this set of points is a set of tetrahedra such that (cf. [17]):

- A point  $\mathbf{z} \in \mathbb{R}^d$  is a vertex of a tetrahedron in  $\mathcal{T}(S)$  only if  $\mathbf{z} \in S$ .

- The intersection of two tetrahedra of  $\mathcal{T}(S)$  is either empty or it is a shared face, a shared edge or a shared vertex.
- The union of all tetrahedra in  $\mathcal{T}(S)$  entirely fulfills the convex hull of  $S$ .

Each  $k$ -simplex is associated with a dual  $(d - k)$ -cell,  $*\sigma^k$ ,  $k \in \{0, 1, 2, 3\}$ . Fig. 1 illustrates this connection. The top row shows primal mesh with one simplex of dimension 0, 1, 2, and 3 (green):  $\sigma^0$  is a vertex,  $\sigma^1$  is an edge,  $\sigma^2$  is a face, and  $\sigma^3$  is a tetrahedron. Their corresponding dual cells  $*\sigma^k$  are shown in red on bottom here restricted to the original primal tetrahedron.

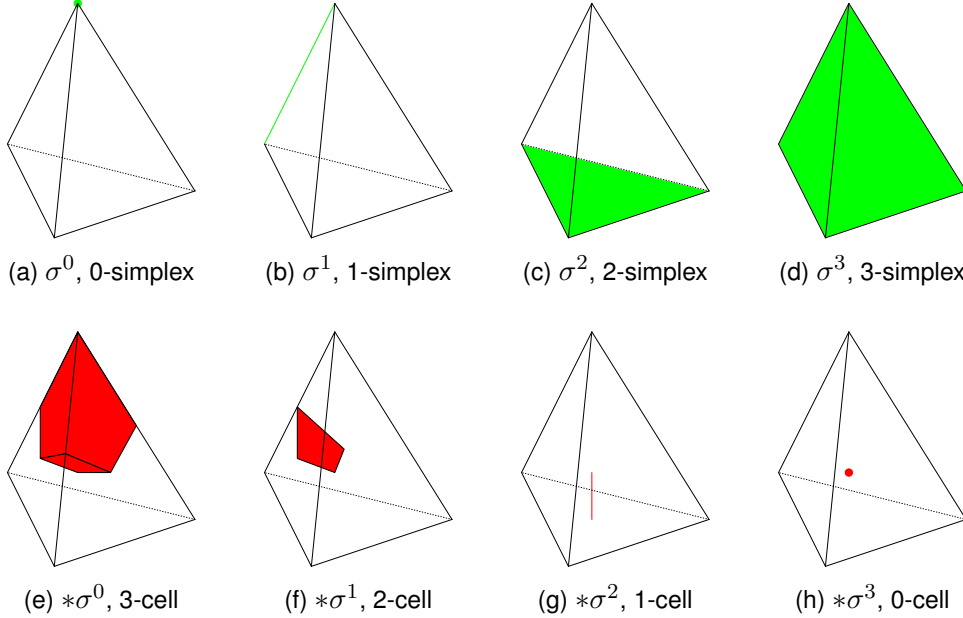


Figure 1: The dual of a triangulation in  $\mathbb{R}^3$ .

The dual of  $\mathcal{T}$  forms a cell complex  $\mathcal{D}$ . A very common dual to a triangulation is the cell complex which uses the circumcenters of each  $d$ -simplex as dual vertices. If the initial triangulation is Delaunay then this dual is simply the Voronoi diagram of the primal vertices. Thus, we obtain a primal-dual triangulation  $(\mathcal{T}, \mathcal{D})$  with the nice properties of non-self-intersection, convexity, and orthogonality of the primal-dual elements (cf. [8]). The Delaunay/Voronoi triangulations  $(\mathcal{T}, \mathcal{D})$  don't allow to change the dual mesh if the primary grid is fixed. This is a restriction. The regular triangulation  $\mathcal{RT}$ , also called a weighted Delaunay triangulation, is a generalization of  $\mathcal{T}$ . Power diagrams  $\mathcal{PD}$ , also called Laguerre or weighted Voronoi diagrams, are the dual structure of regular triangulations. The complex  $(\mathcal{RT}, \mathcal{PD})$  provides orthogonal primal-dual triangulations with much more self-centered simplices  $\sigma^d$ .

Each point  $\mathbf{x}_i \in \mathbb{R}^d$  in  $\mathcal{RT}$  is associated with a real number  $w_i \in \mathbb{R}$ . The real number  $w_i$  is called a weight and  $(\mathbf{x}_i, w_i)$  a weighted point. If the weight  $w_i$  is non-negative, then  $(\mathbf{x}_i, w_i)$  can be interpreted as a sphere centered at the point  $\mathbf{x}_i$  with a radius  $\sqrt{w_i}$ . The power distance of a point  $\mathbf{z} \in \mathbb{R}^d$  with respect to a weighted point  $(\mathbf{x}_i, w_i)$  is defined as

$$\pi_i(\mathbf{z}) = \|\mathbf{z} - \mathbf{x}_i\|^2 - w_i, \quad (4)$$

where  $\|\cdot\|$  denotes the Euclidian distance. It does not matter whether  $\mathbf{z}$  is weighted or un-weighted. The power distance  $\pi_i(\mathbf{z})$  can be interpreted as a square of length of a tangent from the point  $\mathbf{z}$  to a sphere centered at  $\mathbf{x}_i$  and with radius  $\sqrt{w_i}$  if  $\mathbf{z}$  lies outside this sphere. Two weighted points  $(\mathbf{x}_i, w_i)$  and  $(\mathbf{x}_j, w_j)$  are said to be orthogonal if  $\|\mathbf{x}_j - \mathbf{x}_i\|^2 = w_i + w_j$ , i.e.,  $\pi_i(\mathbf{x}_j) = w_j$ . For each weighted point  $(\mathbf{x}_i, w_i)$  with  $\mathbf{x}_i \in S$ , its power cell is defined by

$$\tilde{V}_i = \{\mathbf{z} \in \mathbb{R}^d : \pi_i(\mathbf{z}) \leq \pi_j(\mathbf{z}), \forall \mathbf{x}_j \in S\}. \quad (5)$$

Note that in a regular triangulation, a point  $\mathbf{x}_i \in S$  may not be used in the triangulation because its weighted Voronoi cell is empty, i.e.,  $\mathbf{x}_i$  is not a vertex of  $\mathcal{RT}(S)$  (cf. [8, 17]). There is a close relation between regular triangulations in  $\mathbb{R}^d$  and convex hulls in  $\mathbb{R}^{d+1}$ . The height  $h_i$  of a vertex  $\mathbf{x}_i$  is the  $(d+1)$ -coordinate of  $\mathbf{x}_i^+$  to which it is lifted by the parabolic map, i.e.,  $\mathbf{x}_i^+ = (\mathbf{x}_i, h_i)$ . The weights and heights are related by  $h_i = \|\mathbf{x}_i\|^2 - w_i$  (cf. [11, 17]).

The weighted circumcenter, also called the orthogonal center, of a  $k$ -simplex  $\sigma^k$  is given by the unique intersection of the mutually-orthogonal affine spaces supporting the primal simplex  $\sigma^k$  and its weighted dual  $*\sigma^k$  (cf. [8]). It is denoted  $\mathbf{c}(\sigma^k)$ . In other words,  $\mathbf{c}(\sigma^k)$  is an orthogonal center of  $\sigma^k$  if  $\mathbf{c}(\sigma^k)$  is orthogonal to the  $k+1$  points of  $\sigma^k$ . If  $\mathbf{x}_i$  is any of the vertices of  $\sigma^k$ , the weighted circumcenter is computed by

$$\mathbf{c}(\sigma^k) = \mathbf{x}_i + \frac{1}{2k!|\sigma^k|} \sum_{\mathbf{x}_j \in \sigma^k} (\|\mathbf{x}_i - \mathbf{x}_j\|^2 + w_i - w_j) \hat{\mathbf{n}}_j^k \quad (6)$$

where  $\hat{\mathbf{n}}_j^k$  denotes the inward-pointing normal of the face of  $\sigma^k$  opposite to  $\mathbf{x}_j$  (cf. [8]). For this, the orientation of the  $d$ -simplex  $\sigma^d$ , i.e., the orientation of the set of  $d+1$  points is important. It

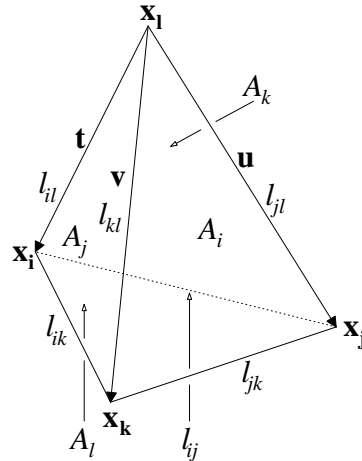


Figure 2: A tetrahedron having positive orientation.

is positive if the points occur in the orientation illustrated in Fig. 2. We can apply a right-hand rule: orient the right hand with fingers curled to follow the circular sequence  $jkl$ . If the thumb points toward  $i$  then  $\sigma^d$  has a positive orientation. In other words, the vectors  $\mathbf{t}, \mathbf{u}$ , and  $\mathbf{v}$ , in

this order, define a positive frame. Using Eq. 6, we obtain for the orthogonal center  $\mathbf{c}_{ijkl}$  the following expression in  $\mathbb{R}^3$  (cf. [11]):

$$\mathbf{c}_{ijkl} = \mathbf{x}_l + \frac{(\|\mathbf{t}\|^2 + w_l - w_i)\hat{\mathbf{n}}_i + (\|\mathbf{u}\|^2 + w_l - w_j)\hat{\mathbf{n}}_j + (\|\mathbf{v}\|^2 + w_l - w_k)\hat{\mathbf{n}}_k}{12|T_{ijkl}|} \quad (7)$$

where  $|T_{ijkl}|$  is the volume of the tetrahedron  $T_{ijkl}$  spanned by the vertices  $\mathbf{x}_i$ ,  $\mathbf{x}_j$ ,  $\mathbf{x}_k$ , and  $\mathbf{x}_l$ . Using  $\mathbf{t} = \mathbf{x}_i - \mathbf{x}_l$ ,  $\mathbf{u} = \mathbf{x}_j - \mathbf{x}_l$ , and  $\mathbf{v} = \mathbf{x}_k - \mathbf{x}_l$ , the outward-pointing and inward-pointing normals are

$$\begin{aligned} \mathbf{n}_i &= \mathbf{v} \times \mathbf{u}, & \hat{\mathbf{n}}_i &= -\mathbf{n}_i = \mathbf{u} \times \mathbf{v}, \\ \mathbf{n}_j &= \mathbf{t} \times \mathbf{v}, & \hat{\mathbf{n}}_j &= -\mathbf{n}_j = \mathbf{v} \times \mathbf{t}, \\ \mathbf{n}_k &= \mathbf{u} \times \mathbf{t}, & \hat{\mathbf{n}}_k &= -\mathbf{n}_k = \mathbf{t} \times \mathbf{u}, \quad \text{and} \\ \mathbf{n}_l &= (\mathbf{x}_i - \mathbf{x}_k) \times (\mathbf{x}_j - \mathbf{x}_k). \end{aligned} \quad (8)$$

An alternative formula for the last vector is  $\mathbf{n}_l = \hat{\mathbf{n}}_i + \hat{\mathbf{n}}_j + \hat{\mathbf{n}}_k$ . A simplex  $\sigma^k$  is said to be self-centered if  $\mathbf{c}(\sigma^k)$  lies in the interior of  $\sigma^k$ .

### 3 Maxwellian grid equations

Given a set of points  $S \subset \mathbb{R}^3$  with  $n_p$  points  $\mathbf{x}_i = \sigma_i^0$ ,  $i = 1, \dots, n_p$ , and associated weights  $w_i \in \mathbb{R}$ . The regular triangulation  $\mathcal{RT}(S)$  consists of  $n_r$  3-simplices (tetrahedra)  $\sigma_i^3$ ,  $i = 1, \dots, n_r$ ,  $n_f$  faces  $A_i = \sigma_i^2$ ,  $i = 1, \dots, n_f$ , and  $n_e$  edges  $L_i = \sigma_i^1$ ,  $i = 1, \dots, n_e$ . The power diagram  $\mathcal{PD}$  consists of  $n_r$  0-cells,  $*\sigma_i^3$ , i.e., the weighted orthogonal centers of  $\sigma_i^3$ , of  $n_f$  edges  $\tilde{L}_i$ ,  $*\sigma_i^2$ ,  $n_e$  faces  $\tilde{A}_i$ ,  $*\sigma_i^1$ , and  $n_p$  3-cells,  $*\sigma_i^0$ .

#### 3.1 Discretization of Maxwell's equations

In the FIT [14, 15, 3, 4], the electric and magnetic voltages and fluxes over the elementary objects of  $\sigma_i^3$  and  $*\sigma_i^0$  are defined as state variables in the following way:

$$e_i = \int_{L_i} \mathbf{E} \cdot d\mathbf{l} \quad h_j = \int_{\tilde{L}_j} \mathbf{H} \cdot d\mathbf{l} \quad (9a)$$

$$d_i = \iint_{\tilde{A}_i} \mathbf{D} \cdot n d\mathbf{A} \quad b_j = \iint_{A_j} \mathbf{B} \cdot n d\mathbf{A} \quad (9b)$$

$$i = 1, \dots, n_e \quad j = 1, \dots, n_f$$

where  $\mathbf{n}$  is the outward-pointing normal of the faces  $A_j$  and  $\tilde{A}_i$ , respectively. The current flux and the electric charge are defined as

$$\begin{aligned} j_i &= \iint_{\tilde{A}_i} \mathbf{J} \cdot n d\mathbf{A} & q_k &= \iiint_{\tilde{V}_k} q dV \\ i &= 1, \dots, n_e & k &= 1, \dots, n_p. \end{aligned} \quad (10)$$

Using Eqs. (9) and (10), the Maxwell's equations (cf. (1)) can then discretized for all the components [16]. Thus, we obtain a compact matrix-vector form:

$$C \mathbf{e} = -\frac{d}{dt} \mathbf{b} \quad \tilde{C} \mathbf{h} = \frac{d}{dt} \mathbf{d} + \mathbf{j} \quad (11a)$$

$$S \mathbf{b} = 0 \quad \tilde{S} \mathbf{d} = \mathbf{q}. \quad (11b)$$

The matrices  $C$ ,  $C := (c_{ij})_{n_f \times n_e}$ , and  $\tilde{C}$ ,  $\tilde{C} := (\tilde{c}_{ij})_{n_e \times n_f}$ , represent the incidence relations between edges and faces on  $\mathcal{RT}$  and  $\mathcal{PD}$ , respectively. Analogously, the matrices  $S$ ,  $S := (s_{ij})_{n_r \times n_f}$ , and  $\tilde{S}$ ,  $\tilde{S} := (\tilde{s}_{ij})_{n_p \times n_e}$ , represent the incidence relations between faces and volumes on  $\mathcal{RT}$  and  $\mathcal{PD}$ , respectively. The matrices  $C$ ,  $\tilde{C}$ ,  $S$ , and  $\tilde{S}$  satisfy the important relations

$$\tilde{C} = C^T, \quad SC = 0, \quad \text{and} \quad \tilde{S}\tilde{C} = 0. \quad (12)$$

### 3.2 Discretization of the constitutive relations

To complete the system of equations (11), the quantities defined on the primary grid and the quantities defined on the dual grid are connected. The usual vector expressions of the constitutive relations (2) involve scalar multiplication. With differential forms, we cannot use these same relations. An Operator that relates forms of different degrees must be introduced. Using the star or Hodge star operator,  $\star$ , the constitutive relations are (cf. [13])

$$D = \varepsilon \star E \quad (13a)$$

$$B = \mu \star H \quad (13b)$$

$$J = \kappa \star E. \quad (13c)$$

The Hodge operator depends on a metric. If the metric is taken to be the permittivity, the permeability, or the conductivity tensor, the constitutive relations (13) become

$$D = M_\varepsilon E \quad (14a)$$

$$B = M_\mu H \quad (14b)$$

$$J = M_\kappa E. \quad (14c)$$

Eqs. (13b) and (14b) can be rewritten as

$$H = \nu \star B \quad \text{and} \quad H = M_\nu B \quad (15)$$

where  $\nu = \mu^{-1}$  is the reluctivity. The matrices  $M_\varepsilon$ ,  $M_\nu$ , and  $M_\kappa$  are generalized material matrices or discrete Hodge operators. They are material and metric dependent and have to be symmetric positive definite.

For an arbitrary primal element  $\sigma$ , the diagonal approximation of the Hodge star of a continuous differential form  $\alpha$  is given by the relation

$$\frac{1}{|\star \sigma|} \int_{\star \sigma} \star \alpha \approx \frac{1}{|\sigma|} \int_{\sigma} \alpha, \quad (16)$$

where  $|\sigma|$  and  $|\ast\sigma|$  are the volumes of these elements (cf. [8, 12]). Let  $\sigma_i^k$  be the  $i$ -th  $k$ -simplex and  $\ast\sigma_i^k$  the dual  $(d - k)$ -cell of the primal-dual triangulation  $(\mathcal{RT}, \mathcal{PD})$ . Then the discrete  $k$ -th Hodge star is a diagonal matrix  $(M^k)_{ii}$  with

$$(M^k)_{ii} = \frac{|\ast\sigma_i^k|}{|\sigma_i^k|}, \quad \forall i. \quad (17)$$

Thus, using (17) we get

$$(M_\varepsilon)_{ii} = \frac{\bar{\varepsilon}\tilde{A}_i}{L_i}, \quad (M_\nu)_{ii} = \frac{\bar{\nu}\tilde{L}_i}{A_i}, \quad \text{and} \quad (M_\kappa)_{ii} = \frac{\bar{\kappa}\tilde{A}_i}{L_i}, \quad (18)$$

where  $\bar{\varepsilon}$  is the face-averaged permittivity,  $\bar{\nu}$  the edge-averaged reluctivity, and  $\bar{\kappa}$  the face-averaged conductivity. If the weighted circumcenter of the any simplex  $\sigma_i^d$  is outside the simplex, i.e.,  $\sigma_i^d$  is not self-centered, then the matrices  $M_\varepsilon$ ,  $M_\nu$ , and  $M_\kappa$  (cf. (18)) are not positive definite. This is an important disadvantage.

For each simplex  $\sigma_i^d$  that is not self-centered we use a locally barycentric dual mesh to make the matrices  $M_\varepsilon$ ,  $M_\nu$ , and  $M_\kappa$  symmetric positive definite. The construction of the constitutive matrices is performed using the microcell method (cf. [4]). The microcell interpolation scheme is a general way to build local constitutive matrices. Microcells are elementary cells with hexahedral shape in the 3d cases. Referring Fig. 3, it is easy to see that each primary tetrahedral cell is divided by the dual edges in four different microcells, one for each of its four nodes. Each microcell belongs, at the same time, to a primary and dual cell. The interpolation method starts from the assumption of a homogeneous medium and a constant field in the microcells (cf. [3, 4]). On every primary element  $V(\equiv T_{ijkl})$ , the consistency condition (20) is always locally satisfied if the following equations are valid:

$$\left. \begin{aligned} LM_\varepsilon^V L^T &= \varepsilon|V| \\ SM_\nu^V S^T &= \nu|V| \\ LM_\kappa^V L^T &= \kappa|V| \end{aligned} \right\} \quad \forall V, \quad (19)$$

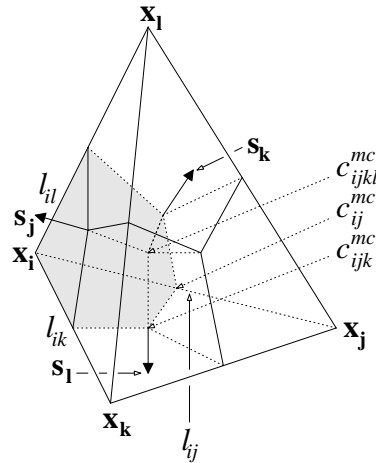


Figure 3: The four microcells of a tetrahedron.

where  $M_\varepsilon^V$ ,  $M_\nu^V$ , and  $M_\kappa^V$  are the material matrices on  $V$  and  $|V|$  is the volume of element  $V$ .  $L$  is a matrix whose columns are the three independent components of the vectors belonging to the primary element  $V$ , i.e., 6 in the case of a tetrahedron.  $S$  is a matrix whose columns are the three independent components of the area vectors belonging to the primary element  $V$ , i.e., 4 in the case of a tetrahedron. The discrete electric energy,  $e^V$ , equals the continuous one,  $\mathbf{E}$ , for a field constant in the cell  $V$ . Same holds for the magnetic energy,  $\mathbf{b}^V$  und  $\mathbf{B}$ .

$$\begin{aligned} L &= [\mathbf{l}_{ij} \mathbf{l}_{ik} \mathbf{l}_{il} \mathbf{l}_{jk} \mathbf{l}_{jl} \mathbf{l}_{kl}] & S &= [\mathbf{s}_i \mathbf{s}_j \mathbf{s}_k \mathbf{s}_l] \\ \mathbf{e}^V &= L^T \mathbf{E}, \quad \mathbf{E} = (E_x, E_y, E_z)^T & \mathbf{b}^V &= S^T \mathbf{B}, \quad \mathbf{B} = (B_x, B_y, B_z)^T \\ (\mathbf{e}^V)^T M_\varepsilon^V \mathbf{e}^V &= & (\mathbf{b}^V)^T M_\nu^V \mathbf{b}^V &= \\ \mathbf{E}^T L M_\varepsilon^V L^T \mathbf{E} &= \mathbf{E}^T \varepsilon |V| \mathbf{E} & \mathbf{B}^T S M_\nu^V S^T \mathbf{B} &= \mathbf{B}^T \nu |V| \mathbf{B} \end{aligned} \quad (20)$$

The matrices  $M_\varepsilon^V$ ,  $M_\nu^V$ , and  $M_\kappa^V$  are assembled out of the following locally defined microcell matrices

$$M_\varepsilon^{V_i} = (L^{V_i})^{-1} \varepsilon (L^{V_i})^{-T} |V_i| \quad (21a)$$

$$M_\nu^{V_i} = (S^{V_i})^{-1} \nu (S^{V_i})^{-T} |V_i| \quad (21b)$$

$$M_\kappa^{V_i} = (L^{V_i})^{-1} \kappa (L^{V_i})^{-T} |V_i| \quad (21c)$$

where  $L^{V_i}$  and  $S^{V_i}$  are  $3 \times 3$  matrices. For the node  $\mathbf{x}_i$  we get

$$L^{V_i} = \begin{pmatrix} l_{ij}(x) & l_{ik}(x) & l_{il}(x) \\ l_{ij}(y) & l_{ik}(y) & l_{il}(y) \\ l_{ij}(z) & l_{ik}(z) & l_{il}(z) \end{pmatrix} \quad \text{and} \quad S^{V_i} = \begin{pmatrix} s_j(x) & s_k(x) & s_l(x) \\ s_j(y) & s_k(y) & s_l(y) \\ s_j(z) & s_k(z) & s_l(z) \end{pmatrix}. \quad (22)$$

$|V_i|$  is the volume of the microcell with  $V_i = [\mathbf{x}_i \ c_{ik}^{mc} \ c_{ijk}^{mc} \ c_{ij}^{mc} \ c_{il}^{mc} \ c_{ikl}^{mc} \ c_{ijkl}^{mc} \ c_{ijl}^{mc}]$  and

$$c_{ijkl}^{mc} = \begin{cases} c_{ijkl} & \text{if } T_{ijkl} \text{ is self-centered} \\ \text{barycenter of } T_{ijkl} & \text{otherwise} \end{cases} \quad (23a)$$

$$c_{ijk}^{mc} = \begin{cases} c_{ijk} & \text{if } T_{ijkl} \text{ is self-centered} \\ c_{ijk} & \text{if } T_{ijkl'} \text{ is self-centered} \\ & (T_{ijkl} \text{ share a face with } T_{ijkl'}) \\ \text{barycenter of triangle } t_{ijk} & \text{otherwise} \end{cases} \quad (23b)$$

$$c_{ij}^{mc} = \begin{cases} c_{ij} & \text{if } T_{ijkl} \text{ is self-centered} \\ c_{ij} & \text{if } T_{ijk'l'} \text{ is self-centered} \\ & (T_{ijkl} \text{ share an edge with } T_{ijk'l'}) \\ \text{barycenter of line } l_{ij} & \text{otherwise.} \end{cases} \quad (23c)$$

Using (21) and (22), we get

$$M_\varepsilon^{V_i} = \begin{pmatrix} m_{\varepsilon 11}^i & m_{\varepsilon 12}^i & m_{\varepsilon 13}^i \\ m_{\varepsilon 21}^i & m_{\varepsilon 22}^i & m_{\varepsilon 23}^i \\ m_{\varepsilon 31}^i & m_{\varepsilon 32}^i & m_{\varepsilon 33}^i \end{pmatrix} \quad \text{and} \quad M_\nu^{V_i} = \begin{pmatrix} m_{\nu 11}^i & m_{\nu 12}^i & m_{\nu 13}^i \\ m_{\nu 21}^i & m_{\nu 22}^i & m_{\nu 23}^i \\ m_{\nu 31}^i & m_{\nu 32}^i & m_{\nu 33}^i \end{pmatrix}. \quad (24)$$

Keeping on this assembling process also with the nodes  $j$ ,  $k$ , and  $l$ , the full primary area material matrices  $M_\varepsilon^V$  and  $M_\nu^V$  may be calculated as follows:

$$M_\varepsilon^V = \begin{pmatrix} m_{\varepsilon 11}^i + & m_{\varepsilon 12}^i & m_{\varepsilon 13}^i & m_{\varepsilon 12}^j & m_{\varepsilon 13}^j & 0 \\ m_{\varepsilon 11}^j & & & & & \\ m_{\varepsilon 21}^i & m_{\varepsilon 22}^i + & m_{\varepsilon 23}^i & m_{\varepsilon 12}^k & 0 & m_{\varepsilon 13}^k \\ & m_{\varepsilon 11}^k & & & & \\ m_{\varepsilon 31}^i & m_{\varepsilon 32}^i & m_{\varepsilon 33}^i + & 0 & m_{\varepsilon 12}^l & m_{\varepsilon 13}^l \\ & & m_{\varepsilon 11}^l & & & \\ m_{\varepsilon 21}^j & m_{\varepsilon 21}^k & 0 & m_{\varepsilon 22}^j + & m_{\varepsilon 23}^j & m_{\varepsilon 23}^k \\ & & & m_{\varepsilon 22}^k & & \\ m_{\varepsilon 31}^j & 0 & m_{\varepsilon 21}^l & m_{\varepsilon 32}^j & m_{\varepsilon 33}^j + & m_{\varepsilon 23}^l \\ & & & & m_{\varepsilon 22}^l & \\ 0 & m_{\varepsilon 31}^k & m_{\varepsilon 31}^l & m_{\varepsilon 32}^k & m_{\varepsilon 32}^l & m_{\varepsilon 33}^k + \\ & & & & & m_{\varepsilon 33}^l \end{pmatrix} \quad (25)$$

and

$$M_\nu^V = \begin{pmatrix} m_{\nu 11}^j + m_{\nu 11}^k & m_{\nu 12}^k + m_{\nu 12}^l & m_{\nu 12}^j + m_{\nu 13}^l & m_{\nu 13}^j + m_{\nu 13}^k \\ +m_{\nu 11}^l & & & \\ m_{\nu 21}^k + m_{\nu 21}^l & m_{\nu 11}^i + m_{\nu 22}^k & m_{\nu 12}^i + m_{\nu 23}^l & m_{\nu 13}^i + m_{\nu 23}^k \\ & +m_{\nu 22}^l & & \\ m_{\nu 21}^j + m_{\nu 31}^l & m_{\nu 21}^i + m_{\nu 32}^l & m_{\nu 22}^i + m_{\nu 22}^j & m_{\nu 23}^i + m_{\nu 23}^j \\ & & +m_{\nu 33}^l & \\ m_{\nu 31}^j + m_{\nu 31}^k & m_{\nu 31}^i + m_{\nu 32}^k & m_{\nu 32}^i + m_{\nu 32}^j & m_{\nu 33}^i + m_{\nu 33}^j \\ & & & +m_{\nu 33}^k \end{pmatrix} \quad (26)$$

where  $m_{\varepsilon mn}^\alpha = m_{\varepsilon nm}^\alpha$  and  $m_{\nu mn}^\alpha = m_{\nu nm}^\alpha$  for  $\alpha \in \{i, j, k, l\}$  and  $m, n \in \{1, 2, 3\}$ . The same applies for the material matrix  $M_\kappa^V$  (cf. (25)). The global matrices  $M_\varepsilon$ ,  $M_\nu$ , and  $M_\kappa$  can be assembled from the local matrices  $M_\varepsilon^V$ ,  $M_\nu^V$ , and  $M_\kappa^V$ .

### 3.3 Linear algebraic equations in the frequency domain

From Sec. 3.1, the equation for the fast varying transient electromagnetic fields is

$$C^T M_\nu C \mathbf{e} + M_\kappa \frac{d}{dt} \mathbf{e} + M_\varepsilon \frac{d^2}{dt^2} \mathbf{e} = 0.$$

If all field quantities vary sinusoidally with time, with angular frequency  $\omega$ , the electric field  $\mathbf{E}(r, t)$  may be written as:

$$\begin{aligned} \mathbf{E}(r, t) &= \mathbf{E}_0(r) \cos(\omega t + \phi(r)) \\ &= \Re(\mathbf{E}_0(r) e^{j(\omega t + \phi(r))}) \\ &= \Re(\mathbf{E}_0(r) e^{j\phi(r)} e^{j\omega t}) \end{aligned} \quad (27)$$

where  $\mathbf{E}_0(r)$  is the amplitude and  $\phi(r)$  the phase. The phasor form in frequency domain is

$$\underline{\mathbf{E}}(r) = \mathbf{E}_0(r) e^{j\phi(r)} \in \mathbb{C}. \quad (28)$$

The electric field  $\mathbf{E}(r, t)$  is obtained from  $\underline{\mathbf{E}}(r)$  by multiplying  $\underline{\mathbf{E}}(r)$  with the time-dependent factor  $e^{j\omega t}$  and taking the real part, i.e.,  $\mathbf{E}(r, t) = \Re(\underline{\mathbf{E}}(r)e^{j\omega t})$ .

Using (9) - (12), (14), and (15) we get Maxwell's equations in phasor form:

$$C\underline{\mathbf{e}} = -j\omega\underline{\mathbf{b}} \quad (29a)$$

$$C^T M_\nu \underline{\mathbf{b}} = j\omega M_\epsilon \underline{\mathbf{e}} + M_\kappa \underline{\mathbf{e}}. \quad (29b)$$

By use of Eq. (29a) in Eq. (29b) we obtain the eigenvalue problem

$$C^T M_\nu C \underline{\mathbf{e}} + j\omega M_\kappa \underline{\mathbf{e}} = \omega^2 M_\epsilon \underline{\mathbf{e}} \quad (30)$$

and without lossy materials ( $M_\kappa = 0$ ) the problem

$$C^T M_\nu C \underline{\mathbf{e}} = \omega^2 M_\epsilon \underline{\mathbf{e}}. \quad (31)$$

Another notation of Eq. (31) is

$$(M_\nu^{1/2} C M_\epsilon^{-1/2})^T (M_\nu^{1/2} C M_\epsilon^{-1/2}) \underline{\mathbf{e}}' = \omega^2 \underline{\mathbf{e}}' \quad \text{with} \quad \underline{\mathbf{e}}' = M_\epsilon^{1/2} \underline{\mathbf{e}}. \quad (32)$$

Using (12), another important property of Eq. (31) is

$$\underbrace{\tilde{S} C^T}_{=0} M_\nu C \underline{\mathbf{e}} = \omega^2 \tilde{S} M_\epsilon \underline{\mathbf{e}} = \omega^2 \tilde{S} \underline{\mathbf{d}} = 0. \quad (33)$$

If  $\omega^2 \neq 0$ , i.e.,  $\tilde{S} \underline{\mathbf{d}} = 0$ , then from Eqs. (31) and (33) we get

$$(C^T M_\nu C + M_\epsilon \tilde{S}^T D_{\tilde{V}}^{-1} \tilde{S} M_\epsilon - \omega^2 M_\epsilon) \underline{\mathbf{e}} = 0 \quad (34)$$

where  $D_{\tilde{V}}$  is the diagonal matrix of dual cell volumes  $\tilde{V}$ , i.e.,  $\star\sigma^0$ , and it is (cf. [5])

$$M_\epsilon \tilde{S}^T D_{\tilde{V}}^{-1} \tilde{S} M_\epsilon \equiv 0.$$

Using Krylov subspace methods, the boundary value problem (34) can be solved iteratively (cf. [9, 10]).

## 4 Hodge-optimized triangulations

It is introduced a family of functionals on pairs of complexes  $(\mathcal{RT}, \mathcal{PD})$  that is derived from bounds on the errors induced by diagonal Hodge stars. The minimizers of these functionals, called HOT meshes [8], can optimize the dual mesh alone to make it more self-centered. It is often enough to find a good non-optimal minimum in order to dramatically improve the mesh quality.

Using Eq. (16) the error density  $e_i$  on the dual of a  $k$ -simplex  $\sigma_i$  is given as the average difference between the discrete approximation and the exact Hodge star:

$$e_i = \frac{1}{|\star\sigma_i|} \left| \frac{|\star\sigma_i|}{|\sigma_i|} \int_{\sigma_i} \alpha - \int_{\star\sigma_i} \star\alpha \right| = \left| \frac{1}{|\sigma_i|} \int_{\sigma_i} \alpha - \frac{1}{|\star\sigma_i|} \int_{\star\sigma_i} \star\alpha \right|. \quad (35)$$

Due to the orthogonality of  $\sigma_i$  and  $\star\sigma_i$ , one can write the integrals of (16) as (cf. [8])

$$\int_{\sigma_i} \alpha = \int_{\sigma_i} f(\mathbf{x}) d\mu_{\sigma_i} \quad \text{and} \quad \int_{\star\sigma_i} \star\alpha = \int_{\star\sigma_i} f(\mathbf{x}) d\mu_{\star\sigma_i}$$

where  $f(\mathbf{x}) : \mathbb{R}^d \rightarrow \mathbb{R}$  is a scalar function and  $d\mu_{\sigma_i}$  and  $d\mu_{\star\sigma_i}$  are volume forms of  $\sigma_i$  and  $\star\sigma_i$ , respectively. With these expressions, one can rewrite the error density (35) as

$$e_i = \left| \int_{\sigma_i} f(\mathbf{x}) \frac{d\mu_{\sigma_i}}{|\sigma_i|} - \int_{\star\sigma_i} f(\mathbf{x}) \frac{d\mu_{\star\sigma_i}}{|\star\sigma_i|} \right| = \left| \int_{\mathbb{R}^d} f(\mathbf{x}) \left( \frac{d\mu_{\sigma_i}}{|\sigma_i|} - \frac{d\mu_{\star\sigma_i}}{|\star\sigma_i|} \right) \right| \quad (36)$$

where  $d\mu_{\sigma_i}/|\sigma_i|$  and  $d\mu_{\star\sigma_i}/|\star\sigma_i|$  are probability distributions over  $\sigma_i$  and  $\star\sigma_i$ , respectively.

The  $q$ -Wasserstein metric, i.e., a common distance function defined between probability distributions in  $\mathbb{R}^d$  with bounded support, is defined as

$$W_q(\mu, \nu) = \left( \inf_{\gamma \in \Gamma(\mu, \nu)} \int_{\mathbb{R}^d \times \mathbb{R}^d} \|\mathbf{x} - \mathbf{y}\|^q d\gamma(\mathbf{x}, \mathbf{y}) \right)^{1/q}.$$

By a direct application of the Hölder inequality we obtain

$$W_1(\mu, \nu) \leq W_2(\mu, \nu). \quad (37)$$

The following dual representation of  $W_1(\mu, \nu)$  is a special case of the duality theorem of Kantorovich and Rubinstein when  $\mu$  and  $\nu$  have bounded support:

$$W_1(\mu, \nu) = \sup_{f: \mathbb{R}^d \rightarrow \mathbb{R}} \left\{ \frac{1}{\lambda} \int_{\mathbb{R}^d} f(\mathbf{x}) d(\mu - \nu) : \text{Lip}(f) \leq \lambda \leq 1 \right\} \quad (38)$$

where  $\text{Lip}(f)$  denotes the minimal Lipschitz constant for  $f$ . From Eq. (36) and Eq. (38) one obtains the relationship

$$e_i \leq \lambda W_1(\sigma_i, \star\sigma_i). \quad (39)$$

This formally establishes a link between optimal transport and approximation error of diagonal Hodge stars. Note it is only required  $\alpha$  to be Lipschitz continuous. Using the  $L_2$  integral norm, one can assemble a total error by summing the error densities  $e_i$  over local regions, specific to  $\sigma_i$  and  $\star\sigma_i$ . These regions denoted as  $\diamond(\sigma_i \cup \star\sigma_i)$  are the convex hulls of  $\sigma_i$  and  $\star\sigma_i$ . Fig. 4 shows these regions, called as support volumes or diamonds, restricted to the original primal tetrahedron (cf. Fig. 1). Thus, the total error is

$$E_2(\mathcal{RT}, \mathcal{PD}, \star^k) = \left( \sum_{\sigma_i^k} \int_{\diamond(\sigma_i^k \cup \star\sigma_i^k)} e_i^2 \right)^{\frac{1}{2}} = \left( \sum_{\sigma_i^k} \frac{|\sigma_i^k| |\star\sigma_i^k|}{\binom{d}{k}} e_i^2 \right)^{\frac{1}{2}}.$$

Due to the orthogonality of  $\mathcal{RT}$  and  $\mathcal{PD}$  the volume of the diamond  $\diamond(\sigma_i^k \cup \star\sigma_i^k)$  equals  $\frac{|\sigma_i^k| |\star\sigma_i^k|}{\binom{d}{k}}$ . Using Eqs. (39) and (37) a tight bound of the total error is expressed as

$$\begin{aligned} E_2(\mathcal{RT}, \mathcal{PD}, \star^k)^2 &\leq \frac{\lambda^2}{\binom{d}{k}} \sum_{\sigma_i^k} |\sigma_i^k| |\star\sigma_i^k| W_1(\sigma_i^k, \star\sigma_i^k)^2 \\ &\leq \frac{1}{\binom{d}{k}} \sum_{\sigma_i^k} |\sigma_i^k| |\star\sigma_i^k| W_2(\sigma_i^k, \star\sigma_i^k)^2 \equiv \star^k - \text{HOT}_{2,2}(\mathcal{RT}, \mathcal{PD}). \end{aligned} \quad (40)$$

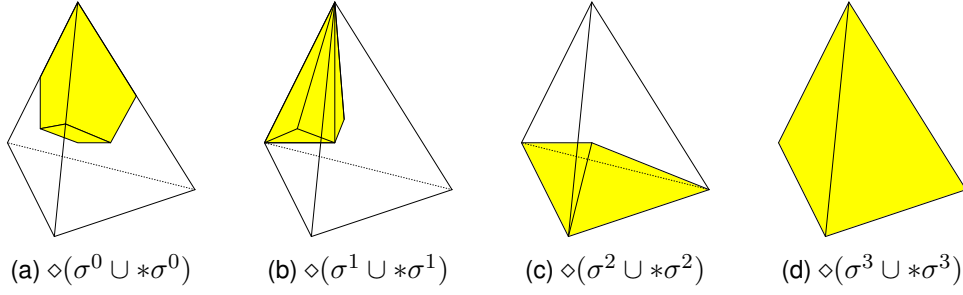


Figure 4: The support volume of a triangulation in  $\mathbb{R}^3$ .

## 4.1 General minimization procedure

A HOT mesh consists of a regular triangulation  $\mathcal{RT}$  and its associated power diagram  $\mathcal{PD}$  for which  $\mathcal{RT}$ ,  $\mathcal{PD}$ , or both have been optimized in order to reduce one HOT functional. Here, if one has a given triangulation, vertices could be held fixed while weights are optimized to better one of the Hodge stars, i.e., Hodge-optimized triangulations can optimize the dual mesh alone. A pseudocode of a general procedure is given in Table 2. This common minimization procedure

Table 2: Basic pseudocode of HOT mesh optimization.

Input: vertices  $\{\mathbf{x}_i\}$  with weights  $\mathbf{w}^0 = \{w_i^0\}$  and  
 $0 \leq k \leq d$  (type of  $\star^k - \text{HOT}_{2,2}(\mathcal{RT}, \mathcal{PD})$ )  
 $n := 0$   
 Compute  $(\mathcal{RT}, \mathcal{PD})$   
**repeat**  
 Compute  $\star^k - \text{HOT}_{2,2}(\mathcal{RT}, \mathcal{PD})$   
 Pick step direction  $\mathbf{d}_w$  for  $\star^k - \text{HOT}_{2,2}(\mathcal{RT}, \mathcal{PD})$   
 Find  $\beta$  satisfying Wolfe conditions  
 $\mathbf{w}^{n+1} := \mathbf{w}^n + \beta \mathbf{d}_w$   
 $n := n + 1$   
 Update  $(\mathcal{RT}, \mathcal{PD})$   
**until** (convergence criterion met)

works without anything else but an evaluation of a HOT energy and its gradient which will derive in closed form from direct integration.

In the unconstrained minimization problem, the Wolfe conditions are a set of inequalities for performing inexact line search. The basic problem is to solve

$$\min_{\mathbf{x} \in \mathbb{R}^n} f(\mathbf{x})$$

for some smooth  $f : \mathbb{R}^n \rightarrow \mathbb{R}$ . In line search algorithm the sequence  $\{\mathbf{x}_k\}$  is constructed iteratively at each step choosing a search direction  $\mathbf{p}_k$ . Thus, the objective function is minimized along the line in this direction. This reduced the problem to a sequence of one dimensional

problems

$$\min_{\gamma \in \mathbb{R}} f(\mathbf{x}_k + \gamma \mathbf{p}_k)$$

with the step length  $\gamma > 0$ . A step length  $\gamma_k$  is said to satisfy the Wolfe conditions if the following two inequalities hold:

- 1  $f(\mathbf{x}_k + \gamma_k \mathbf{p}_k) \leq f(\mathbf{x}_k) + c_1 \gamma_k \mathbf{p}_k^T \nabla f(\mathbf{x}_k)$   
(Armijo rule, sufficient decrease)
- 2  $\mathbf{p}_k^T \nabla f(\mathbf{x}_k + \gamma_k \mathbf{p}_k) \geq c_2 \mathbf{p}_k^T \nabla f(\mathbf{x}_k)$   
(curvature condition)

with  $0 < c_1 < c_2 < 1$  and  $\mathbf{p}_k = -\nabla f(\mathbf{x}_k)$ . This ensures that  $\mathbf{p}_k$  is a descent direction, i.e.,  $\mathbf{p}_k^T \nabla f(\mathbf{x}_k) < 0$ . The solution of the minimization problem occurs without updating the complex  $(\mathcal{RT}, \mathcal{PD})$ .

## 4.2 HOT<sub>2,2</sub> energies

The HOT<sub>2,2</sub> energies can be expressed as a function of signed distances between the weighted circumcenters of  $k$ - and  $(k + 1)$ -simplices with  $0 \leq k \leq d - 1$  (cf. Fig. 5). The weighted

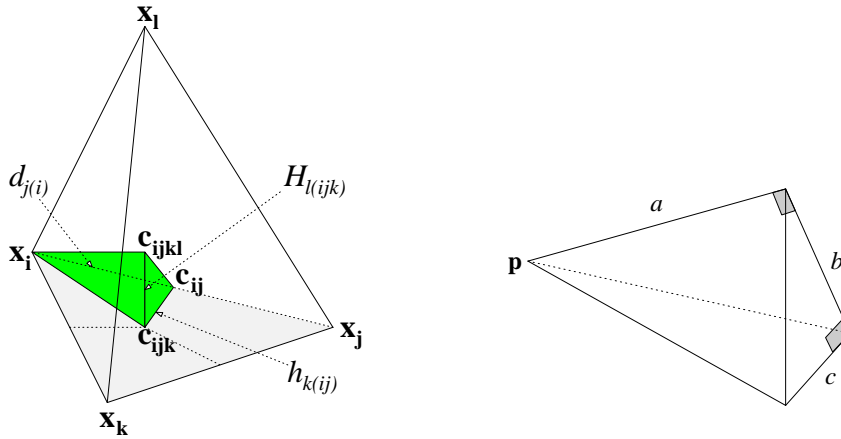


Figure 5: Signed distances between circumcenters.

circumcenter of the  $k$ -simplex  $\sigma^k$  is the orthogonal projection of the weighted circumcenter of the  $(k + 1)$ -simplex  $\sigma^{k+1}$  onto simplex  $\sigma^k$ . The signed distance from the weighted circumcenter of  $\sigma^{k+1}$ ,  $c_{k+1}$ , to the weighted circumcenter of  $\sigma^k$  has a positive distance if the simplices  $\sigma^{k+1}$  and  $\{\sigma^k, c_{k+1}\}$  have the same orientation, and negative otherwise.

For both  $\star^0$  and  $\star^d$ , HOT<sub>2,2</sub> energies can be easily computed by splitting  $d$ -cells  $\star^0$  or primal  $d$ -simplices  $\sigma^d$  into canonical subsimplices for which closed form integral expressions  $W(\mathbf{p}, T)$  are found.  $T$  is a tetrahedron spanned by the edges  $a$ ,  $b$ , and  $c$  and vertex  $\mathbf{p}$  is adjacent to edge

$a$  (cf. Fig. 5). The other remaining stars are just combinations of transport over edges, areas, and volumes. So here one can find closed form integral expressions  $W(a, t)$  for an edge  $a$  and the triangle  $t$  spanned by the edges  $b$  and  $c$ . Using the squared distance (cf. Eq. (37)), in Eq. (40) the integral expressions  $W(\mathbf{p}, T)$  and  $W(a, t)$  are given by:

$$\begin{aligned} W(\mathbf{p}, T) &= \int_0^a \int_0^{\frac{b}{a}x} \int_0^{\frac{c}{b}y} (x^2 + y^2 + z^2) dz dy dx \\ &= \frac{1}{5} \left( \frac{a^3 bc}{2} + \frac{ab^3 c}{4} + \frac{abc^3}{12} \right), \end{aligned} \quad (41a)$$

$$\begin{aligned} W(a, t) &= \frac{1}{3} \left( \frac{bc}{2} \int_0^a x^2 dx + a \int_0^b \int_0^{\frac{c}{b}y} (y^2 + z^2) dz dy \right) \\ &= \frac{1}{3} \left( \frac{a^3 bc}{6} + \frac{ab^3 c}{4} + \frac{abc^3}{12} \right). \end{aligned} \quad (41b)$$

For the subsimplex given in Fig. 5 we obtain the following relations for the  $\text{HOT}_{2,2}$  energies.

$\star^0 - \text{HOT}_{2,2}$	$\star^1 - \text{HOT}_{2,2}$	$\star^2 - \text{HOT}_{2,2}$	$\star^3 - \text{HOT}_{2,2}$
$W(\mathbf{p}, T)$	$W(a, t)$	$W(a, t)$	$W(\mathbf{p}, T)$
$\mathbf{p} \leftarrow \mathbf{x}_i$			$\mathbf{p} \leftarrow \mathbf{c}_{ijkl}$
$a \leftarrow d_{j(i)}$			$a \leftarrow H_{l(ijk)}$
$b \leftarrow h_{k(ij)}$			$b \leftarrow h_{k(ij)}$
$c \leftarrow H_{l(ijk)}$			$c \leftarrow d_{j(i)}$

Using the integral forms of  $W(\mathbf{p}, T)$  (Eq. (41a)) and  $W(a, t)$  (Eq. (41b)), all the  $\text{HOT}_{2,2}$  energies for every tetrahedron  $T_{ijkl}$  are expressed as a function of the signed distances  $d_{j(i)}$ ,  $h_{k(ij)}$ , and  $H_{l(ijk)}$  between circumcenters as follows:

$$\begin{aligned} \star^0 - \text{HOT}_{2,2}(T_{ijkl}) &= \\ &= \sum_r \sum_s \sum_t \frac{1}{5} \left( \frac{H_{r(stu)}^3 h_{s(tu)} d_{t(u)}}{12} + \frac{H_{r(stu)} h_{s(tu)}^3 d_{t(u)}}{4} + \frac{H_{r(stu)} h_{s(tu)} d_{t(u)}^3}{2} \right) \end{aligned}$$

$$\begin{aligned} \star^1 - \text{HOT}_{2,2}(T_{ijkl}) &= \\ &= \sum_r \sum_s \sum_t \frac{1}{3} \left( \frac{H_{r(stu)}^3 h_{s(tu)} d_{t(u)}}{12} + \frac{H_{r(stu)} h_{s(tu)}^3 d_{t(u)}}{4} + \frac{H_{r(stu)} h_{s(tu)} d_{t(u)}^3}{6} \right) \end{aligned}$$

$$\begin{aligned} \star^2 - \text{HOT}_{2,2}(T_{ijkl}) &= \\ &= \sum_r \sum_s \sum_t \frac{1}{3} \left( \frac{H_{r(stu)}^3 h_{s(tu)} d_{t(u)}}{6} + \frac{H_{r(stu)} h_{s(tu)}^3 d_{t(u)}}{4} + \frac{H_{r(stu)} h_{s(tu)} d_{t(u)}^3}{12} \right) \end{aligned}$$

$$\star^3 -\text{HOT}_{2,2}(T_{ijkl}) = \sum_r \sum_s \sum_t \frac{1}{5} \left( \frac{H_{r(stu)}^3 h_{s(tu)} d_{t(u)}}{2} + \frac{H_{r(stu)} h_{s(tu)}^3 d_{t(u)}}{4} + \frac{H_{r(stu)} h_{s(tu)} d_{t(u)}^3}{12} \right)$$

where the indices  $r, s, t$ , and  $u$  are determined by  $r \in \{i, j, k, l\}$ ,  $s \in \{i, j, k, l\} \setminus \{r\}$ ,  $t \in \{i, j, k, l\} \setminus \{r, s\}$ , and  $u \in \{i, j, k, l\} \setminus \{r, s, t\}$ . The arrangement of the indices  $s, t$ , and  $u$  of  $H_{r(stu)}$  and  $t$  and  $u$  of  $h_{s(tu)}$ , respectively is not of any importance. Every permutation of  $\{s, t, u\}$  yields the same distance  $H_{r(\dots)}$ . The same applies to  $\{t, u\}$  and  $h_{s(\dots)}$ . Thus, the total error (40) is computed by

$$E_2(\mathcal{RT}, \mathcal{PD}, \star^k)^2 = \sum_{T_{ijkl}} \star^k - \text{HOT}_{2,2}(T_{ijkl}).$$

Using Eq. (4), we have

$$\begin{aligned} d_{j(i)}^2 - w_i &= d_{i(j)}^2 - w_j \\ &= (\ell_{ij} - d_{j(i)})^2 - w_j \\ &= \ell_{ij}^2 - 2\ell_{ij}d_{j(i)} + d_{j(i)}^2 - w_j \end{aligned}$$

with  $\ell_{ij} = \|x_j - x_i\|$ .

Thus, we get

$$d_{j(i)} = \frac{\ell_{ij}^2 + w_i - w_j}{2\ell_{ij}} \quad (42)$$

for the signed distance between  $\mathbf{c}_i (= \mathbf{x}_i)$  and  $\mathbf{c}_{ij}$ . Denoting by  $h_{k(ij)}$  the signed distance between  $\mathbf{c}_{ij}$  and  $\mathbf{c}_{ijk}$  in a triangle  $t_{ijk}$  we get

$$h_{k(ij)} = \frac{d_{k(i)} - d_{j(i)} \cos \gamma_i}{\sin \gamma_i}$$

where  $\gamma_i$  is the angle at  $\mathbf{x}_i$  in triangle  $t_{ijk}$  (cf. Fig. 6). Applying the traditional Hodge star  $(\star^1)_{ij}$  for a 1-form between vertex  $i$  and vertex  $j$  in a regular triangulation (cf. [8]), we obtain

$$h_{k(ij)} = \frac{\ell_{ij} \cot \gamma_k}{2} + \frac{w_j \cot \gamma_i + w_i \cot \gamma_j}{2\ell_{ij}} - \frac{w_k \ell_{ij}}{4|t_{ijk}|}. \quad (43)$$

$H_{l(ijk)}$  is the signed distance between  $\mathbf{c}_{ijk}$  and  $\mathbf{c}_{ijkl}$  in tetrahedron  $T_{ijkl}$  (cf. Eq. (8)):

$$\begin{aligned} H_{l(ijk)} &= (\mathbf{c}_{ijk} - \mathbf{c}_{ijkl}) \cdot \frac{(\mathbf{x}_i - \mathbf{x}_k) \times (\mathbf{x}_j - \mathbf{x}_k)}{\|(\mathbf{x}_i - \mathbf{x}_k) \times (\mathbf{x}_j - \mathbf{x}_k)\|} \\ &= \begin{cases} \|\mathbf{c}_{ijk} - \mathbf{c}_{ijkl}\| & \text{if } \mathbf{x}_i \text{ and } \mathbf{c}_{ijkl} \text{ lie in the same half-plane,} \\ -\|\mathbf{c}_{ijk} - \mathbf{c}_{ijkl}\| & \text{otherwise.} \end{cases} \end{aligned} \quad (44)$$

The weight optimization of each  $\text{HOT}_{2,2}$  energy can easily be done using the derivatives of Eq. (42)

$$\frac{\partial d_{j(i)}}{\partial w_i} = \frac{1}{2\ell_{ij}}, \quad \frac{\partial d_{j(i)}}{\partial w_j} = -\frac{1}{2\ell_{ij}},$$

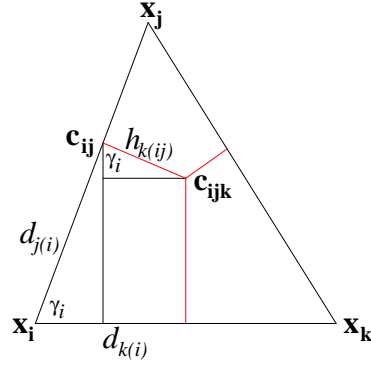


Figure 6: The signed distance between weighted edge and triangle circumcenter.

and the derivatives of Eq. (43)

$$\frac{\partial h_{k(ij)}}{\partial w_i} = \frac{\cot \gamma_j}{2\ell_{ij}}, \quad \frac{\partial h_{k(ij)}}{\partial w_j} = \frac{\cot \gamma_i}{2\ell_{ij}}, \quad \frac{\partial h_{k(ij)}}{\partial w_k} = -\frac{\ell_{ij}}{4|t_{ijk}|}.$$

The derivative of the weighted circumcenter with respect to the weights can be easily computed. Using Eq. (6), the derivatives at vertex  $\mathbf{x}_1$  result in

$$\frac{\partial \mathbf{c}_{ijk}}{\partial w_r} = \frac{1}{4|t_{ijk}|} \mathbf{n}_r^2, \quad \frac{\partial \mathbf{c}_{ijk}}{\partial w_i} \equiv 0, \quad \text{and} \quad \frac{\partial \mathbf{c}_{ijk}}{\partial w_s} = \frac{1}{12|T_{ijkl}|} \mathbf{n}_s^3$$

where  $r \in \{i, j, k\}$ ,  $s \in \{i, j, k, l\}$ , and  $\mathbf{n}_r^2$  and  $\mathbf{n}_s^3$  denote the outward normals of the triangle  $t_{ijk}$  and of the tetrahedron  $T_{ijkl}$ , respectively. From Eq. (44), we obtain

$$\begin{aligned} \frac{\partial H_{l(ijk)}}{\partial w_s} &= \left( \frac{\partial \mathbf{c}_{ijk}}{\partial w_s} - \frac{\partial \mathbf{c}_{ijkl}}{\partial w_s} \right) \cdot \frac{(\mathbf{x}_i - \mathbf{x}_k) \times (\mathbf{x}_j - \mathbf{x}_k)}{\|(\mathbf{x}_i - \mathbf{x}_k) \times (\mathbf{x}_j - \mathbf{x}_k)\|} \\ &= \begin{cases} \frac{(\mathbf{c}_{ijk} - \mathbf{c}_{ijkl})}{\|\mathbf{c}_{ijk} - \mathbf{c}_{ijkl}\|} \cdot \left( \frac{\partial \mathbf{c}_{ijk}}{\partial w_s} - \frac{\partial \mathbf{c}_{ijkl}}{\partial w_s} \right) & \text{if } \mathbf{x}_1 \text{ and } \mathbf{c}_{ijkl} \text{ lie in the same half-plane,} \\ -\frac{(\mathbf{c}_{ijk} - \mathbf{c}_{ijkl})}{\|\mathbf{c}_{ijk} - \mathbf{c}_{ijkl}\|} \cdot \left( \frac{\partial \mathbf{c}_{ijk}}{\partial w_s} - \frac{\partial \mathbf{c}_{ijkl}}{\partial w_s} \right) & \text{otherwise.} \end{cases} \end{aligned}$$

Because the normal  $\frac{(\mathbf{x}_i - \mathbf{x}_k) \times (\mathbf{x}_j - \mathbf{x}_k)}{\|(\mathbf{x}_i - \mathbf{x}_k) \times (\mathbf{x}_j - \mathbf{x}_k)\|}$  is perpendicular to the derivatives  $\frac{\partial \mathbf{c}_{ijk}}{\partial w_s}$ ,  $s \in \{i, j, k, l\}$ , the corresponding scalar products are equal to zero. The same applies for the normal  $\frac{(\mathbf{c}_{ijk} - \mathbf{c}_{ijkl})}{\|\mathbf{c}_{ijk} - \mathbf{c}_{ijkl}\|}$ .

Thus we obtain the following formulas:

$$\begin{aligned}\frac{\partial H_{l(ijk)}}{\partial w_i} &= -\frac{1}{12|T_{ijkl}|} \mathbf{n}_i^3 \cdot \frac{(\mathbf{x}_i - \mathbf{x}_k) \times (\mathbf{x}_j - \mathbf{x}_k)}{\|(\mathbf{x}_i - \mathbf{x}_k) \times (\mathbf{x}_j - \mathbf{x}_k)\|}, \\ \frac{\partial H_{l(ijk)}}{\partial w_j} &= -\frac{1}{12|T_{ijkl}|} \mathbf{n}_j^3 \cdot \frac{(\mathbf{x}_i - \mathbf{x}_k) \times (\mathbf{x}_j - \mathbf{x}_k)}{\|(\mathbf{x}_i - \mathbf{x}_k) \times (\mathbf{x}_j - \mathbf{x}_k)\|}, \\ \frac{\partial H_{l(ijk)}}{\partial w_k} &= -\frac{1}{12|T_{ijkl}|} \mathbf{n}_k^3 \cdot \frac{(\mathbf{x}_i - \mathbf{x}_k) \times (\mathbf{x}_j - \mathbf{x}_k)}{\|(\mathbf{x}_i - \mathbf{x}_k) \times (\mathbf{x}_j - \mathbf{x}_k)\|}, \\ \frac{\partial H_{l(ijk)}}{\partial w_l} &= -\frac{1}{12|T_{ijkl}|} \|(\mathbf{x}_i - \mathbf{x}_k) \times (\mathbf{x}_j - \mathbf{x}_k)\|.\end{aligned}$$

The normal  $\frac{(\mathbf{x}_i - \mathbf{x}_k) \times (\mathbf{x}_j - \mathbf{x}_k)}{\|(\mathbf{x}_i - \mathbf{x}_k) \times (\mathbf{x}_j - \mathbf{x}_k)\|}$  can be replaced by  $\pm \frac{(\mathbf{c}_{ijk} - \mathbf{c}_{ijkl})}{\|\mathbf{c}_{ijk} - \mathbf{c}_{ijkl}\|}$ , i.e.,

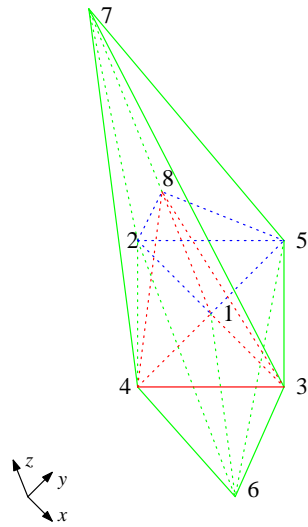
$$\begin{aligned}\frac{\partial H_{l(ijk)}}{\partial w_i} &= \mp \frac{1}{12|T_{ijkl}|} \mathbf{n}_i^3 \cdot \frac{(\mathbf{c}_{ijk} - \mathbf{c}_{ijkl})}{\|\mathbf{c}_{ijk} - \mathbf{c}_{ijkl}\|}, \\ \frac{\partial H_{l(ijk)}}{\partial w_j} &= \mp \frac{1}{12|T_{ijkl}|} \mathbf{n}_j^3 \cdot \frac{(\mathbf{c}_{ijk} - \mathbf{c}_{ijkl})}{\|\mathbf{c}_{ijk} - \mathbf{c}_{ijkl}\|}, \\ \frac{\partial H_{l(ijk)}}{\partial w_k} &= \mp \frac{1}{12|T_{ijkl}|} \mathbf{n}_k^3 \cdot \frac{(\mathbf{c}_{ijk} - \mathbf{c}_{ijkl})}{\|\mathbf{c}_{ijk} - \mathbf{c}_{ijkl}\|}, \\ \frac{\partial H_{l(ijk)}}{\partial w_l} &= \mp \frac{1}{12|T_{ijkl}|} \mathbf{n}_l^3 \cdot \frac{(\mathbf{c}_{ijk} - \mathbf{c}_{ijkl})}{\|\mathbf{c}_{ijk} - \mathbf{c}_{ijkl}\|}.\end{aligned}$$

## 5 Numerical results

We consider two academic examples to demonstrate the generality of the approach. The ability to optimize weights to improve the dual structure is very useful. The first example has the form of a crystal (cf. Fig. 7). The second example is a rectangular bar that is crossed by another bar (cf. Fig. 8). The primal triangular mesh is generated using REGTET, a Fortran program for computing a regular tetrahedralization for a finite set of weighted points in 3d space (cf. [1, 2]). It is based on an algorithm by Edelsbrunner and Shah for constructing regular tetrahedralizations with incremental topological flipping (cf. [6]). The colored areas in the both figures represent different material parameters.

For the first example (cf. Fig. 7) we define a rectangular regular grid on the surface of a rectangular polyhedron that contains the set of input points  $\{\mathbf{x}_1, \dots, \mathbf{x}_8\}$  to become, together with this set of input points, the set for which a tetrahedralization is to be computed. For  $n_{add} \geq 2$  for each facet of the polyhedron a set of  $n_{add} \times n_{add}$  points is generated. This set defines a rectangular regular grid and contains the four vertices of the facet. The union of the six sets thus generated define the rectangular grid on the surface of the polyhedron with  $n_{pol}$  points:

$$n_{pol} = 6(n_{add} - 2)^2 + 12(n_{add} - 2) + 8 = 6n_{add}^2 - 12n_{add} + 8.$$



$$\begin{aligned} \mathbf{x}_1 &= (0.0, 0.0, 0.0) \\ \mathbf{x}_2 &= (-1.0, 0.0, 0.0) \\ \mathbf{x}_3 &= (1.0, 0.0, 0.0) \\ \mathbf{x}_4 &= (0.0, -1.0, 0.0) \\ \mathbf{x}_5 &= (0.0, 1.0, 0.0) \\ \mathbf{x}_6 &= (-0.5, -0.5, -1.0) \\ \mathbf{x}_7 &= (0.0, 0.0, 2.0) \\ \mathbf{x}_8 &= (0.0, 0.0, 1.0) \end{aligned}$$

	$w_i$ at first	$w_i$ finished
1	0.00	-0.016097
2	0.00	0.500195
3	0.00	0.752207
4	0.00	0.497853
5	0.00	0.752421
6	0.00	0.730471
7	0.00	1.819437
8	0.00	0.021272

Figure 7: The crystal.

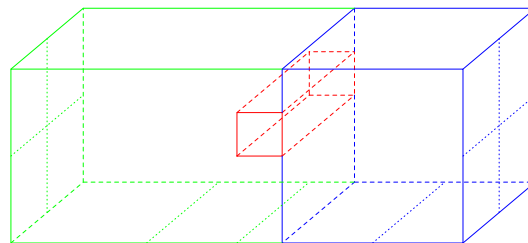


Figure 8: A rectangular bar that is crossed by another rectangular bar.

In Table 3 #tet denotes the number of all tetrahedra and #sctet the number of self-centered tetrahedra. For the first example in Table 3 the weights of the input points and the weights of the points on the surface of the rectangular polyhedron are  $w_i = 0.00$ . The finished weights for  $n_{add} = 0$  at the end of the iteration are given in Fig. 7. This set of weights is not unique. However the number of self-centered tetrahedra has increased significantly.

Table 3: The number of self-centered tetrahedra for  $\star^3 - \text{HOT}_{2,2}$ .

$n_{add}$	$(\mathcal{T}, \mathcal{D})$			$(\mathcal{RT}, \mathcal{PD})$ at first			$(\mathcal{RT}, \mathcal{PD})$ finished		
	#tet	#sctet	%	#tet	#sctet	%	#tet	#sctet	%
first example									
0	12	0	0.00	12	0	0.00	12	10	83.33
2	48	0	0.00	48	0	0.00	46	18	39.13
3	96	14	14.58	96	14	14.58	90	64	71.11
4	170	50	29.41	170	50	29.41	170	117	68.82
5	277	48	17.33	277	48	17.33	278	217	78.06

While the weights of the input points in Table 4 are also  $w_i = 0.00$ , the weights on the surface are  $w_i = 1.00$ . The iterative behavior between  $w_i = 0.00$  and  $w_i = 1.00$  on the surface of the polyhedron is different.

Table 4: The number of self-centered tetrahedra for  $\star^3 - \text{HOT}_{2,2}$  in dependence of the weights on the surface points.

$n_{add}$	$(\mathcal{RT}, \mathcal{PD})$ at first			$(\mathcal{RT}, \mathcal{PD})$ finished		
	#tet	#sctet	%	#tet	#sctet	%
first example						
0	12	0	0.00	12	10	83.33
2	48	0	0.00	47	19	40.43
3	98	15	15.31	89	67	75.28
4	167	46	27.54	166	117	70.48
5	275	22	8.00	263	199	75.67

For the second example, in Table 5 are shown the numbers of self-centered tetrahedra in dependence of the weights of the input points. The weights of the input points are changed as a function of the terms

$$\begin{aligned}
 & i \pmod{8} \cdot 0.100, \\
 & i \pmod{8} \cdot 0.105, \\
 \text{and } & i \pmod{9} \cdot 0.080
 \end{aligned}$$

respectively. Also in this example, the iterative behavior is different in dependence of the weights of the input points.

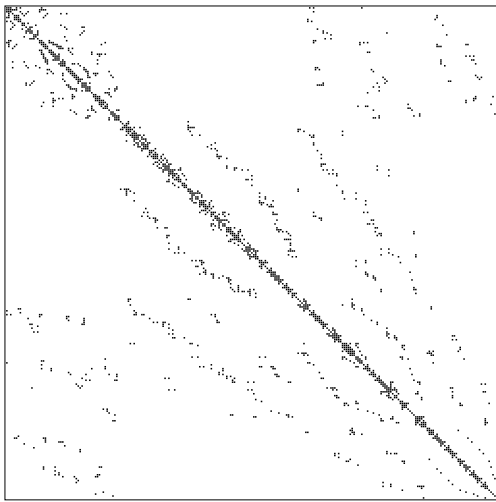
Table 5: The number of self-centered tetrahedra for  $\star^3 - \text{HOT}_{2,2}$  in dependence of the weights of the input points.

$(\mathcal{T}, \mathcal{D})$			$(\mathcal{RT}, \mathcal{PD})$ at first			$(\mathcal{RT}, \mathcal{PD})$ finished			$w_i$
#tet	#sctet	%	#tet	#sctet	%	#tet	#sctet	%	
second example									
144	4	2.78	144	4	2.78	144	109	75.69	0.000
			141	48	34.04	142	106	74.65	$i \pmod{8} \cdot 0.100$
			141	47	33.33	143	115	80.42	$i \pmod{8} \cdot 0.105$
			144	36	25.00	138	93	67.93	$i \pmod{9} \cdot 0.080$

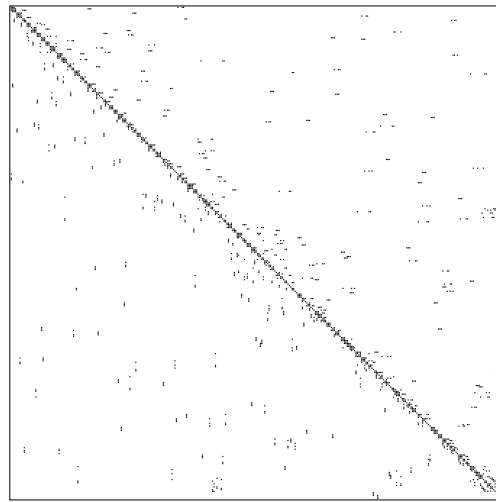
The greater flexibility in the location of dual vertices affects the non-zero pattern of the material matrices (14) (cf. Sec. 3.2). For the second example, this matrices are shown in Fig. 9 with no weights of input points. The dimensions of the material matrices  $M_\varepsilon$  and  $M_\mu$  are denoted by  $n_e$  and  $n_f$ , respectively. The term  $n_{nz}$  represents the number of non-zero elements in  $M_\varepsilon$  and  $M_\mu$ , respectively. The number of non-zero elements of the material matrices  $M_\varepsilon$  and  $M_\mu$  is important reduced. This will affect the calculation of the solution of the systems of linear algebraic equations.

## 6 Conclusions

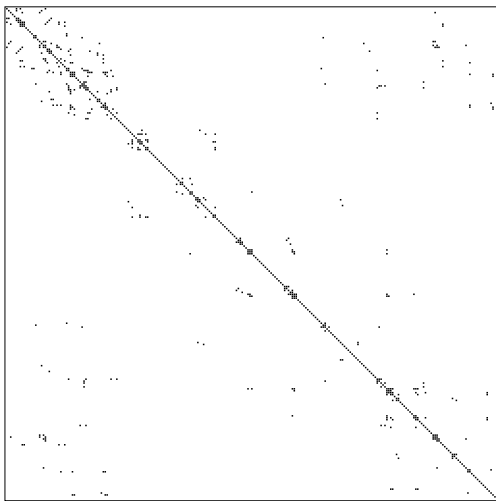
A combination of a mainly orthogonal and locally barycentric mesh is used to discretize the Maxwell's equations in integral form using FIT. For this, we define differential forms of various degrees and identify them with field intensity, flux density, and charge density. The constitutive relations are discretized by using the Hodge star operator. It relates differential forms of different degrees. The duality between regular triangulations and power diagrams allows a different choice on the dual mesh once the primal mesh is fixed. For each tetrahedron that is not self-centered we construct the constitutive matrices by using the microcell method. To reduce the number of non-self-centered tetrahedra we use a mesh based on Hodge-optimized triangulations. This optimization strategy makes more self-centered tetrahedra and thus improved one or more of the discrete Hodge stars. Due to efficiency reasons the set of weights is a non-optimal minimum. However the number of non-zero elements of the material matrices is important reduced. An open problem is the construction of the inverse of the material matrix for the permittivity in order to solve the systems of linear algebraic equations.



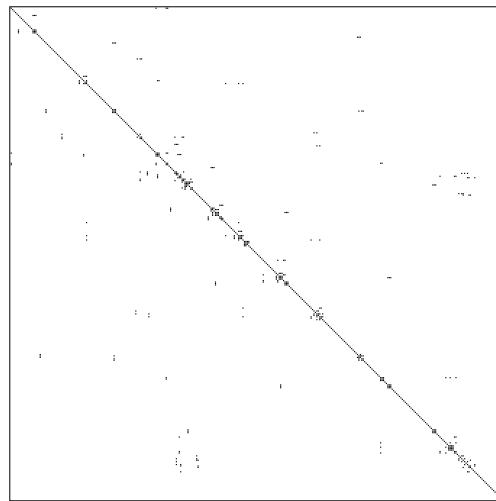
(a)  $M_\varepsilon$  (at first):  $n_e = 255, n_{nz} = 1829$



(b)  $M_\varepsilon$  (finished):  $n_e = 255, n_{nz} = 695$



(c)  $M_\nu$  (at first):  $n_f = 340, n_{nz} = 1834$



(d)  $M_\nu$  (finished):  $n_f = 340, n_{nz} = 714$

Figure 9: The non-zero pattern of matrices  $M_\varepsilon$  and  $M_\nu$ .

## References

- [1] Javier Bernal. Lexicographical manipulations for correctly computing regular tetrahedralizations with incremental topological flipping. NISTIR 6335, 1999.
- [2] Javier Bernal. REGTET: A program for computing regular tetrahedralizations. NISTIR 6786, 2001.
- [3] M. Cinalli, F. Edelvik, R. Schumann, and T. Weiland. Consistent material operators for tetrahedral grids based on geometrical principles. *International Journal of Numerical Modelling: Electronic Networks, Devices and Fields*, 17(5):487–507, 2004.

- [4] Marco Cinalli and Andrea Schiavoni. A stable and consistent generalization of the FDTD technique to nonorthogonal unstructured grids. *IEEE Transactions on Antennas and Propagations*, 54(5):1503–1512, 2006.
- [5] M. Clemens and T. Weiland. Discrete electromagnetism with the finite integration technique. *Progress In Electromagnetics Research*, 32:65–87, 2001.
- [6] H. Edelsbrunner and N.R. Shah. Incremental topological flipping works for regular triangulations. *Algorithmica*, 15(3):223–241, 1996.
- [7] A. Gillette. Notes on discrete exterior calculus. Technical report, University of Texas at Austin, 2009.
- [8] Patrick Mullen, Pooran Memari, Fernando Goes, and Mathieu Desbrun. HOT: Hodge-optimized triangulations. *ACM Transactions on Graphics*, 30(4), 2011.
- [9] Rainer Schlundt, Franz-Josef Schückerle, and Wolfgang Heinrich. Shifted linear systems in electromagnetics. Part I: Systems with identical right-hand sides. WIAS Preprint No. 1420, Weierstraß-Institut für Angewandte Analysis und Stochastik, 2009.
- [10] Rainer Schlundt, Franz-Josef Schückerle, and Wolfgang Heinrich. Shifted linear systems in electromagnetics. Part II: Systems with multiple right-hand sides. WIAS Preprint No. 1646, Weierstraß-Institut für Angewandte Analysis und Stochastik, 2011.
- [11] Jonathan Richard Shewchuk. Lecture notes on geometric robustness. University of California at Berkeley, 2013.
- [12] A. Stern, Y. Tong, M. Desbrun, , and J.E. Marsden. Geometric computational electrodynamics with variational integrators and discrete differential forms. arXiv:0707.4470v3 [math.NA], 2009.
- [13] K.F. Warnick, R.H. Selfridge, and D.V. Arnold. Teaching electromagnetic field theory using differential forms. *IEEE Transactions on Education*, 40, No. 1:53–68, 1997.
- [14] T. Weiland. A discretization method for the solution of Maxwell’s equations for six-component fields. *Electronics and Communication (AEÜ)*, 31:116–120, 1977.
- [15] T. Weiland. On the unique numerical solution of Maxwellian eigenvalue problems in three dimensions. *Particle Accelerators (PAC)*, 17:277–242, 1985.
- [16] T. Weiland. Time domain electromagnetic field computation with finite difference methods. *International Journal of Numerical Modelling: Electronic Networks, Devices and Fields*, 9(4):295–319, 1996.
- [17] Michal Zemek. Regular triangulation in 3d and its applications. Technical Report No. DCSE/TR-2009-03, University of West Bohemia, 2009.